# Linear Response Functions of a Cumulus Ensemble to Temperature and Moisture Perturbations and Implications for the Dynamics of Convectively Coupled Waves

ZHIMING KUANG

*Department of Earth and Planetary Sciences, and School of Engineering and Applied Sciences, Harvard University, Cambridge, Massachusetts*

(Manuscript received 16 July 2009, in final form 24 November 2009)

ABSTRACT

An approach is presented for the construction of linear response functions of a cumulus ensemble to large-scale temperature and moisture perturbations using a cloud system–resolving model (CSRM). A set of time-invariant, horizontally homogeneous, anomalous temperature and moisture tendencies is added, one at a time, to the forcing of the CSRM. By recording the departure of the equilibrium domain-averaged temperature and moisture profiles from those of a control experiment and through a matrix inversion, a sufficiently complete and accurate set of linear response functions is constructed for use as a parameterization of the cumulus ensemble around the reference mean state represented by the control experiment.

This approach is applied to two different mean state conditions in which the CSRM, when coupled with 2D gravity waves, exhibits interestingly different behaviors. With a more strongly convecting mean state forced by the large-scale vertical velocity profile taken from the Tropical Ocean and Global Atmosphere Coupled Ocean–Atmosphere Response Experiment (TOGA COARE), spontaneous development of convectively coupled waves requires moisture variations above the boundary layer, whereas with a mean state of radiative–convective equilibrium (RCE) not forced by large-scale vertical advection, the development of convectively coupled waves is stronger and persists even when moisture variations above the boundary layer are removed. The linear response functions were able to reproduce these behaviors of the full CSRM with some quantitative accuracy. The linear response functions show that both temperature and moisture perturbations at a range of heights can regulate convective heating. The ability for convection to remove temperature anomalies, thus maintaining convective neutrality, decreases considerably from the lower troposphere to the middle and upper troposphere. It is also found that the response of convective heating to a lower tropospheric temperature anomaly is more top-heavy in the RCE case than in the TOGA COARE case. Comparing the linear response functions with the treatment of convection in an earlier simple model by the present author indicates general consistency, lending confidence that the instability mechanisms identified in that model provide the correct explanation to the instability seen in the CSRM simulations and the instability's dependence on the mean state.

## 1. Introduction

Deep cumulus convection plays a key role in the climate system. Understanding and representing how its behavior varies with its large-scale environment is a major challenge in meteorology. While cumulus convection involves many nonlinear, undifferentiable processes, the statistics of the whole cumulus ensemble are expected to be smooth functions of its large-scale environment. Linear response functions to small perturbations in the large-scale environment can therefore be a useful probe of the behavior of the cumulus ensemble around a reference state.

Such linear response functions are particularly relevant to convectively coupled waves. These waves are an important form of the large-scale organization of moist convection, both theoretically and practically [see, e.g., the recent review by Kiladis et al. (2009) for an account of their many implications]. In addition to the extensive observational studies that documented these waves (e.g., Takayabu 1994; Wheeler and Kiladis 1999; Straub and Kiladis 2002; Haertel and Kiladis 2004), cloud system–resolving models (CSRMs) have been shown to reproduce them with good realism (e.g., Grabowski and Moncrieff 2001; Kuang et al. 2005; Peters and Bretherton 2006; Tulich et al. 2006; Kuang 2008a, hereafter K08a; Nasuno

*Corresponding author address:* Zhiming Kuang, Department of Earth and Planetary Sciences, and School of Engineering and Applied Sciences, Harvard University, 20 Oxford St., Cambridge, MA 02138.
E-mail: kuang@fas.harvard.edu

DOI: 10.1175/2009JAS3260.1

et al. 2008; Tulich and Mapes 2008). Over the years, a number of conceptual/toy models of convectively coupled waves have been proposed (e.g., Lindzen 1974; Emanuel 1987; Neelin et al. 1987; Neelin and Yu 1994; Emanuel et al. 1994; Mapes 2000; Fuchs and Raymond 2002; Khouider and Majda 2006; Raymond and Fuchs 2007; Kuang 2008b, hereafter K08b). To make a thorough analysis of these models tractable, they employ simple and highly idealized treatments of convection, and often of the dry dynamics as well. While available observations and CSRM simulations are in general used to inform the conceptual/toy models, the connection is often indirect. The idealized nature of the toy models also makes it difficult to ascertain that the conceptual/toy models truly capture the dynamics of the observed waves and those in the CSRM simulations.

There have been a number of CSRM studies that have looked at the issue of convective response to perturbations to its environment (e.g., Tompkins and Craig 1998; Redelsperger et al. 2002; Derbyshire et al. 2004; Takemi et al. 2004). For example, Takemi et al. (2004) systematically varied the moisture and stratification at a number of altitudes through nudging and examined the equilibrium response in convection. Tulich and Mapes (2010) and the author (see appendix) have independently examined the transient responses of a CSRM to selected temperature and moisture perturbations of the domain mean sounding. In this work, we shall use a new approach to construct a sufficiently complete and accurate set of response functions and use them as a distilled version of the CSRM for coupling with large-scale waves. As we will show, these linear response functions can reproduce the convectively coupled waves simulated by the CSRM with good quantitative accuracy and therefore adequately represent the sensitivities of the cumulus ensemble to large-scale temperature and moisture perturbations. Comparing these response functions with the toy models then helps to ascertain the extent to which they provide the correct explanation of the CSRM simulations.

We will first describe the procedure that we use to construct the linear response functions (section 2). The model and the experimental setups are briefly described in section 3. We then describe simulations with the full CSRM coupled with 2D gravity waves for two different reference mean states, which produced interestingly different behavior. The linear response functions are constructed for these two cases and shown to reproduce the behavior of the full CSRM with good fidelity (section 4). We then discuss the main features of the linear response functions (section 5), compare them to an existing conceptual/toy model (section 6), present additional discussion (section 7), and conclude with a brief summary of the main results (section 8).

## 2. Method for constructing the linear response functions

Our goal is to derive a matrix $\mathbf{M}$ so that, given the anomalous state vector $\mathbf{x}$, we can compute the anomalous convective tendencies as

$$\frac{d\mathbf{x}}{dt} = \mathbf{M}\mathbf{x}. \tag{1}$$

The state vector is considered here to include profiles of domain-averaged temperature $T$ and specific humidity $q$ anomalies (or their projections onto a set of basis functions). Horizontal winds[1] are excluded here but could be included in future studies. Equation (1) assumes that the domain-averaged temperature and moisture profiles completely describe the system; that is, statistics of the cumulus ensemble are unique functions of the domain-averaged temperature and moisture profiles. This is reasonable for waves with periods of days or longer for which $T$ and $q$ vary sufficiently slowly so that the cumulus ensemble can be considered in statistical equilibrium with its large-scale environment at all times.[2]

A natural approach to computing $\mathbf{M}$ is perhaps to introduce, one at a time, a set of horizontally uniform $T$ and $q$ perturbations to a CSRM that is in a statistical equilibrium state and observe how the perturbations evolve with time. However, this approach, while intuitive and offering useful insights, has a number of complications. First, when a perturbation is first added to the CSRM, the cumulus ensemble is not in equilibrium with its large-scale environment, violating the assumption made in Eq. (1). As convection adjusts toward statistical equilibrium with its environment, the domain-averaged $T$ and $q$ profiles are also evolving. The assumption made in Eq. (1) thus cannot be justified for $T$ and $q$ anomalies that evolve on time scales shorter or comparable to the convective response time, which is roughly a few hours. Moreover, the CSRM has a considerable amount of internal noise such that the evolution of domain-averaged $T$ and $q$ can have a sizable stochastic component. As $T$ and $q$ profiles evolve with time, the amount of time averaging available for reducing the stochastic component is limited, and ensemble simulations with large ensemble sizes are necessary to obtain sufficient accuracy.

[1] Large-scale vertical wind is not included because unlike horizontal winds, which directly affect convection through the effect of shear, large-scale vertical wind affects convection indirectly through its effects on temperature and humidity.

[2] It is useful to distinguish two different adjustment times: 1) the time that it takes for the cumulus ensemble to adjust to statistical equilibrium with its large-scale sounding and 2) the time for perturbations to the large-scale sounding (i.e., $\mathbf{x}$) to adjust/decay, which is characterized by the eigenvalues of $\mathbf{M}$.

For the above reasons, we use a different approach in which we force the model with a set of anomalous temperature and moisture tendencies, one at a time. When the model reaches a new equilibrium, the anomalous convective tendencies $d\mathbf{x}/dt$ are just those that balance the prescribed tendencies. The departure of the new equilibrium $T$ and $q$ from the control provides estimates of $\mathbf{x}$. In this approach, the cumulus ensemble is in statistical equilibrium with the large-scale state, as demanded by Eq. (1). In so doing, we neglect the finite response time of convection. Repeating the calculation for all components of $\mathbf{x}$ produces a matrix equation

$$\mathbf{Y} = \mathbf{MX}, \tag{2}$$

where matrix $\mathbf{Y}$ consists of column vectors that are the anomalous convective tendencies and matrix $\mathbf{X}$ consists of column vectors that are estimates of $\mathbf{x}$. Since the computation of $\mathbf{M}$ involves the inverse of $\mathbf{X}$, changes in the eigenvalue of $\mathbf{M}$ (denoted as $\lambda$) due to errors in $\mathbf{X}$ scale as $|\delta\lambda| \propto |\lambda^2|\|\delta\mathbf{X}\|$, where $\|\delta\mathbf{X}\|$ is a matrix norm of the errors in $\mathbf{X}$. This implies that uncertainties in $\mathbf{x}$ ($d\mathbf{x}/dt$ is precisely known here) influence the fast decaying eigenmodes the most, while eigenmodes that decay more slowly are less subject to uncertainties in $\mathbf{x}$. This is a desirable property since for coupling with large-scale waves, especially long period waves, the slowly decaying modes are of the most interest and best preserved. The fast-decaying eigenmodes decay so quickly that they tend not to couple with the large-scale waves as effectively, so errors in these modes are less consequential. Finally, with this approach one can take long time averages to reduce the stochastic noise so that there is no need to make large numbers of ensembles. Practically, this proves to be convenient. We shall adopt this approach while keeping in mind that the finite response time of convection is neglected here, as assumed in Eq. (1). We present a brief comparison of the evolution of $T$ and $q$ anomalies computed from this approach and those from the initial perturbation approach (both without coupling with large-scale waves) in the appendix. The results are qualitatively similar except for a delay of a couple of hours in the initial perturbation case owing to the response time of convection. We have found it easier to achieve accuracies necessary for the present purpose with the prescribed forcing approach.

## 3. Model and experimental setup

The model that we use is the System for Atmospheric Modeling (SAM) version 6.4. A description of an earlier version of this model is given in Khairoutdinov and Randall (2003). The model solves the anelastic equations of motion. The prognostic thermodynamic variables are the liquid water static energy, total nonprecipitating water, and total precipitating water. We use a bulk microphysics scheme and a simple Smagorinsky-type scheme to parameterize the effect of subgrid-scale turbulence. We compute the surface fluxes using a bulk aerodynamic formula with constant exchange coefficients and a constant surface wind speed of 5 m s$^{-1}$ to eliminate any wind-induced surface heat exchange effect. The surface temperature is set to 29.5°C. For the experiments in this paper, unless noted otherwise, the domain size is 128 km × 128 km in the horizontal with a 2-km horizontal resolution. There are 64 vertical points that extend from the surface to 32 km. The vertical grid is the same as that used in K08a.

Two mean states are used in this study. One is that studied in K08a, where we set the domain mean vertical velocity profile to be the mean vertical velocity profile over the Large-Scale Array (LSA) during the intensive observation period (IOP) of the Tropical Ocean Global Atmosphere Coupled Ocean–Atmosphere Response Experiment (TOGA COARE) (Webster and Lukas 1992), as shown in Fig. 1 of K08a. The second mean state is that of a radiative–convective equilibrium (RCE) for which the domain mean vertical velocity is set to zero. In each of the two cases, the model is run with prescribed radiative cooling profiles obtained by first running the respective cases to a statistical equilibrium with interactive radiation, using the National Center for Atmospheric Research Community Atmospheric Model (CAM) radiation package. The use of prescribed radiative cooling eliminates any radiative feedback.

To reduce the computational cost, instead of perturbing the model layer by layer, we use a set of basis functions with coarser vertical resolutions. The basis functions take a Gaussian form

$$\exp\left[-\left(\frac{p - p_s + (i - 1/2)\Delta p}{\Delta p}\right)^2\right],$$

where $p$ is pressure, $p_s$ is the surface pressure, $\Delta p$ = 75 hPa, and $i = 1, 2, \ldots$. We add an extra basis function near the surface, which takes the form of

$$\exp\left[-\left(\frac{p - p_s}{30\ \text{hPa}}\right)^2\right].$$

These basis functions are used for both $T$ and $q$. For $q$, $i$ is capped at 10, which peaks at 295 hPa. For $T$, $i$ is capped at 11 (peaking at 220 hPa) for the RCE case and 12 (peaking at 145 hPa) for the TOGA COARE case because the convective layer is somewhat deeper in the latter case. These functions are chosen empirically so

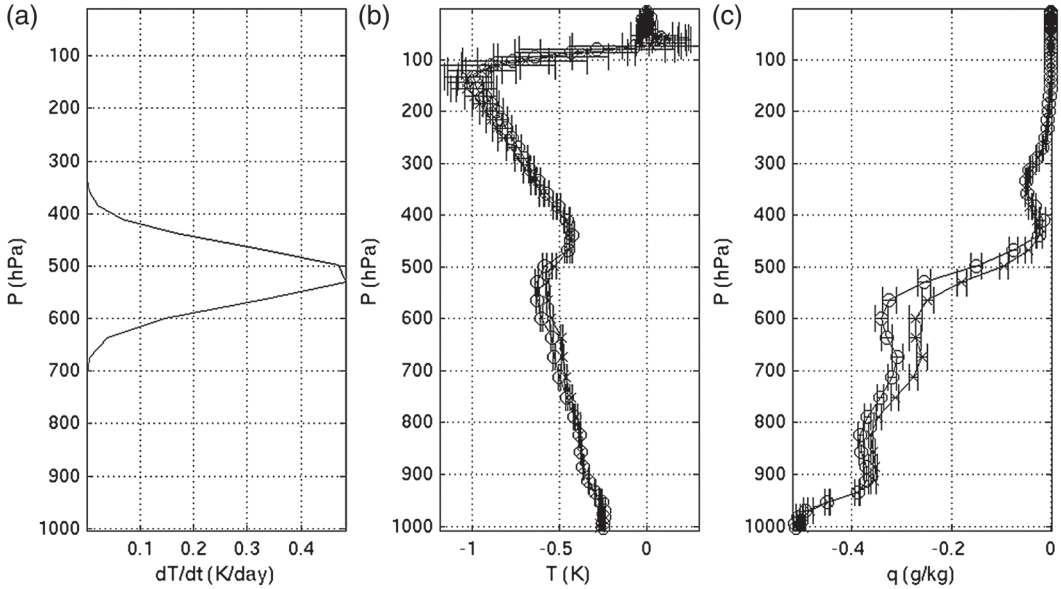


FIG. 1. An example of the temperature (b) and moisture (c) anomalies that are in equilibrium with an anomalous convective heating profile shown in (a) and zero convective moistening tendencies everywhere.

that tropospheric temperature and moisture variations seen in convectively coupled waves simulated with this CSRM can be adequately captured as their linear combinations; no systematic effort, however, was made to minimize the number of basis functions.

For each of the basis functions we perform two runs: one with a positive forcing and the other with a negative forcing. The peak magnitude of the forcing is 0.5 K day$^{-1}$ for temperature and 0.2 g kg$^{-1}$ day$^{-1}$ for specific humidity. The magnitudes are halved for basis functions that peak above 500 hPa and halved again for those that peak above 250 hPa. We first run the model to statistical equilibrium before introducing the forcing. The model is then run for another 200 days, and the last 150 days are averaged and compared to the control simulation to give the anomalous state vector. A typical example is shown in Fig. 1, which shows the temperature (Fig. 1b) and specific humidity (Fig. 1c) anomalies that are in statistical equilibrium with an anomalous convective heating, shown in Fig. 1a, and zero anomalous moisture tendency everywhere. Estimates from both a positive forcing experiment (circles) and negative forcing experiment (crosses) are shown. The uncertainty estimates are given by the standard deviation divided by the square root of the effective sample size, which takes into account the autocorrelation of the time series. Agreement (or disagreement) in the results from the positive and negative forcing experiments gives some indication of the degree of nonlinearity. The agreement seen in Fig. 1 is typical. There are occasional cases of larger disagreement, which can be reduced by halving the forcings. Such fine-tuning does not affect the results reported in this paper and will not be discussed further. Overall, these comparisons indicate that the statistics of the cumulus ensemble respond approximately linearly to sizable perturbations and the linear response functions will be relevant to convectively coupled waves with realistic amplitudes. As a side note, the broad resemblance of the $T$, $q$ anomalies to a shift toward a colder moist adiabat and a drier condition holds for other forcing patterns as well. As will be discussed in section 5, such a pattern represents the slowest decaying eigenmode of $\mathbf{M}$, which is amplified in the equilibrium responses. To form matrix $\mathbf{M}$, we further combine results from the positive and negative forcing experiments, which cancels the quadratic terms in the Taylor expansion and improves the accuracy. The results are then projected onto the basis functions through a linear regression that minimizes the squared residue, which is weighted by the mass of each layer divided by the estimated uncertainty.

Repeating the above for all the basis functions gives matrices $\mathbf{X}$ and $\mathbf{Y}$ in Eq. (2), and matrix $\mathbf{M}$ is then computed. As the fastest decaying modes are most prone to error, often there is an eigenvalue with a large positive real component. Since the CSRM equilibrium state is evidently stable in the absence of feedbacks from the large-scale flow, all eigenmodes are expected to decay so we simply reverse the sign of this eigenvalue and reconstruct the matrix $\mathbf{M}$. As reasoned earlier and confirmed by tests, coupling with large-scale waves is not sensitive to the treatment of this fast decaying mode as long as its sign is corrected so that it is not fast growing.

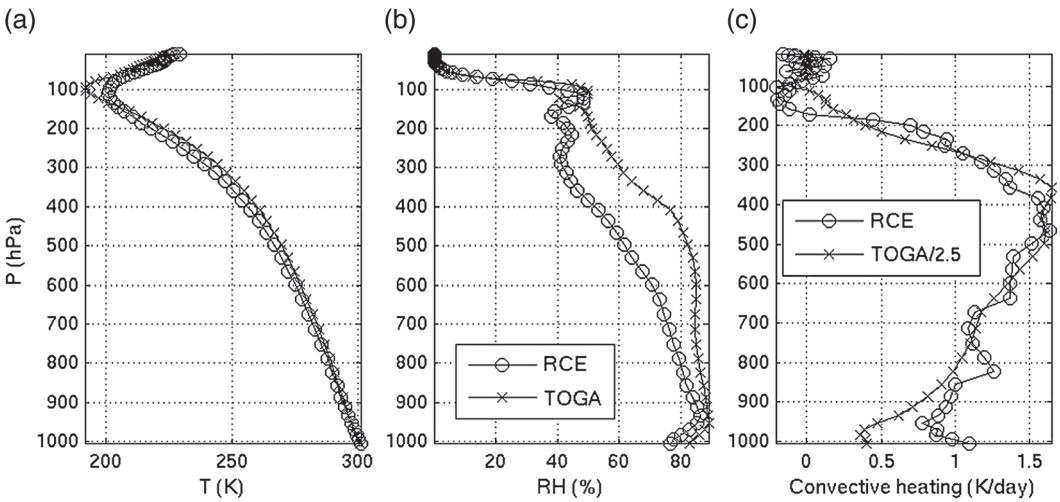


FIG. 2. Comparisons of the RCE (circles) and TOGA COARE (crosses) mean states: (a) temperature, (b) relative humidity, and (c) convective heating. The mean convective heating of the TOGA COARE case has been divided by a factor of 2.5.

## 4. Application to the TOGA COARE and RCE mean states

In this section, we apply our method to the TOGA COARE and RCE cases. The mean states of the two cases are compared in Fig. 2. The mean state of the TOGA COARE case has higher relative humidity. Its stratification is stronger in the lower and middle troposphere but weaker in the upper troposphere. In Fig. 2c, we have reduced the convective heating of the TOGA COARE case by a factor of 2.5 to account for the fact its mean precipitation is about 2.5 times that of the RCE case (9.1 versus 3.6 mm day$^{-1}$). We will first present results from coupling the CSRM to large-scale 2D gravity waves under these mean state conditions and then show that the linear response functions can reproduce these results. The method of coupling the cumulus ensemble with gravity waves is that used in K08a, and readers are referred to that paper for details on the methodology. Briefly, we treat the limited domain CSRM as a vertical line in the 2D gravity wave and make use of the linearity of the problem and model the coupling for a single horizontal wavenumber at a time. In this case, the wave vertical velocity can be evolved based on the CSRM domain-averaged (virtual) temperature anomalies, and the effect of the wave vertical velocity on the cumulus ensemble can be included as additional vertical advection tendencies in the CSRM. This allows for two-way coupling between the large-scale wave and the cumulus ensemble. In addition to the mechanical damping that is included in K08a, we add a thermal damping of the same strength so that an increase in wave damping simply reduces the wave growth rate by a commensurate amount. This way we can vary the damping coefficient and observe when the waves cease to develop and better quantify the strength of the instability.

As in K08a, the model is initialized with equilibrium soundings from earlier runs and spun up for 30 days without wave coupling. The reference mean state is computed by averaging over the last 10 days of this period. Wave coupling is activated on day 30. Unless noted otherwise, a horizontal wavelength of 5000 km is used in the experiments presented below.

Figure 3a shows the spontaneous development of convectively coupled waves for the TOGA COARE case, as shown in K08a. A wave damping time scale of 10 days is applied to the large-scale gravity wave. The composite wave structures are shown in Fig. 4. In the experiment shown in Fig. 3b, we keep the specific humidity above 1 km constant, which is a more appropriate test of whether moisture variations in the free troposphere are important for the wave development than removing vertical advection of moisture by the large-scale waves, as done in K08a. Wave growth is absent in this case even though wave damping is reduced to 1/(1000 days). The remaining fluctuations are forced by stochastic noise from the CSRM. These results confirm the conclusions in K08a and the earlier results by Grabowski and Moncrieff (2004) that convectively coupled waves can spontaneously develop only in the presence of free tropospheric moisture variations.

The same experiments for the RCE case, however, yield different results (Fig. 5). In the control simulation (Fig. 5a), the wave development is considerably stronger than in the TOGA COARE case. A 1.2-day wave damping was used in the experiment to control

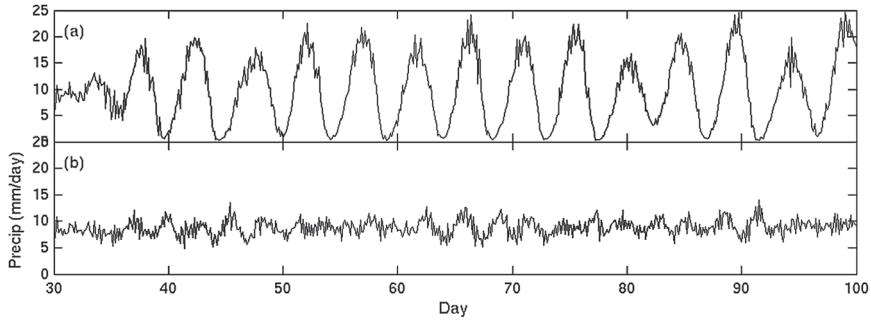


FIG. 3. Domain-averaged precipitation as a function of time after coupling to a large-scale gravity wave is activated for the TOGA COARE case: (a) the control case with a 10-day wave damping and (b) the case with domain-averaged specific humidity kept constant and a 1000-day wave damping. A horizontal wavelength of 5000 km is used.

the wave growth. Damping of this magnitude is found to eliminate wave development in the TOGA COARE control case. Furthermore, when we remove moisture fluctuations above 1 km, convectively coupled waves still develop, even though the growth is weaker than in the control case (a 3-day damping is used in Fig. 5b). The phase speed in this case is faster, ~20 m $s^{-1}$ instead of ~14 m $s^{-1}$ as in the control case. The composite

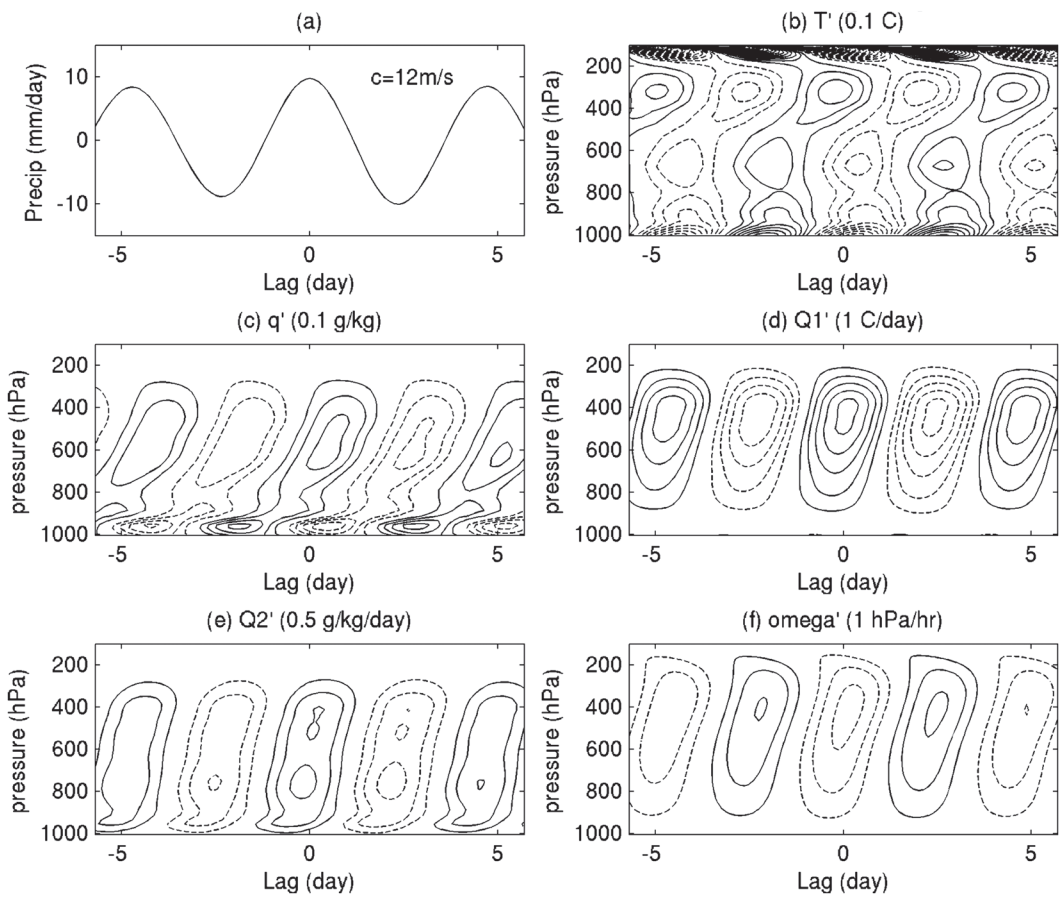


FIG. 4. Composite wave structures for the TOGA COARE control case and a horizontal wavelength of 5000 km: (a) precipitation, (b) temperature, (c) specific humidity, (d) convective heating, (e) convective drying, and (f) vertical pressure velocity. Contour intervals are indicated above each plot. Negative contours are dashed and the zero contours are omitted. The estimated phase speed is shown in (a).

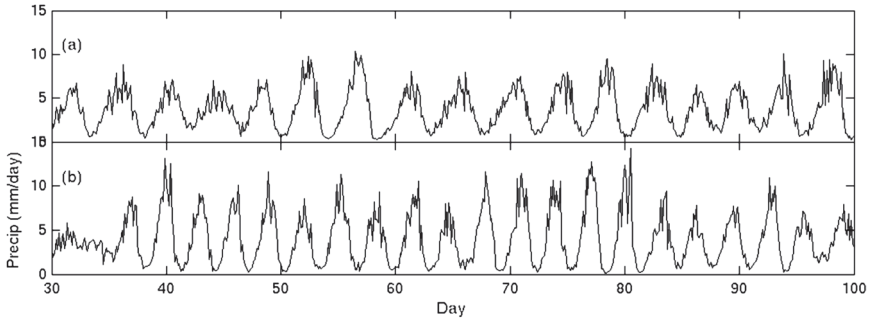


FIG. 5. As in Fig. 3 but for the RCE case: a 1.2-day wave damping is used in (a) and a 3-day wave damping in (b).

wave structures for these two cases are shown in Figs. 6 and 7.

The above results indicate that there exist two different instability mechanisms: one that involves moisture variations in the free troposphere and one that does not. The instability involving free tropospheric moisture appears to be present with either mean state, as evidenced by the weakening or disappearance of wave growth when moisture variations in the free troposphere are removed. On the other hand, the instability mechanism that does not involve free tropospheric moisture seems to be effective only with the RCE mean state.

We now present results from simulations in which the full CSRM is replaced by the linear response function matrix **M**. Coupling with the large-scale gravity wave is the same except that the convective tendencies are now computed using Eq. (1) instead of the CSRM. The runs are initialized with random noises in $T$ and $q$. Figures 8–11 show results from representative periods for the four cases discussed earlier. Since these results are completely linear, they are presented with the same scales as in the earlier figures for their corresponding cases. The linear response functions appear to capture the basic behaviors seen in Figs. 3–7. The TOGA COARE control case (Fig. 8) shows development of unstable waves with a phase speed of 14 m s$^{-1}$. A 20-day wave damping is applied to approximately neutralize the wave growth. With free troposphere (>1 km) specific humidity kept constant, the TOGA COARE case shows no wave growth even though wave damping is set to zero (Fig. 9). The RCE control case (Fig. 10) has the strongest wave growth; a 1.7-day wave damping was needed to approximately neutralize the wave growth. The phase speed is 17 m s$^{-1}$. Wave growth remains but is weakened in the RCE case when free troposphere specific humidity is kept constant (an 8-day wave damping is used to neutralize the wave growth) and the phase speed is 20 m s$^{-1}$, faster than that in the control case. Compared with the results with the full CSRM, results with the linear response functions appear to show slightly weaker wave growth and the cases with free tropospheric moisture variations tend to have slightly faster phase speeds, indicating inaccuracies in the linear response functions. We have found that differences of such magnitude are sensitive to small changes in the linear response functions. However, the basic differences among the four difference cases are robustly captured by the linear response functions and the wave structures also compare sufficiently well with those from the full CSRM for us to conclude that the CSRM can be distilled into these response functions, as far as coupling with linear large-scale waves is concerned. We have also experimented with running the TOGA COARE response functions with the RCE mean $T$, $q$ profiles and vice versa. The results show that, when free troposphere specific humidity is allowed to vary, the RCE background profiles are more favorable for wave growth because of the greater vertical moisture gradient. This effect, however, is secondary compared to those due to differences in the response functions.

## 5. Main characteristics of the response functions

We now examine the main characteristics of the response functions and will compare them with a simple conceptual model in the next section.

Figures 12 and 13 show the anomalous convective tendencies associated with representative temperature and specific humidity anomalies for both the RCE and the TOGA COARE cases. Since the mean precipitation of the TOGA COARE case is about 2.5 times that in the RCE case, the scales for the tendencies of the TOGA COARE case are made 2.5 times those of the RCE case.

The main features of the linear response functions are summarized below.

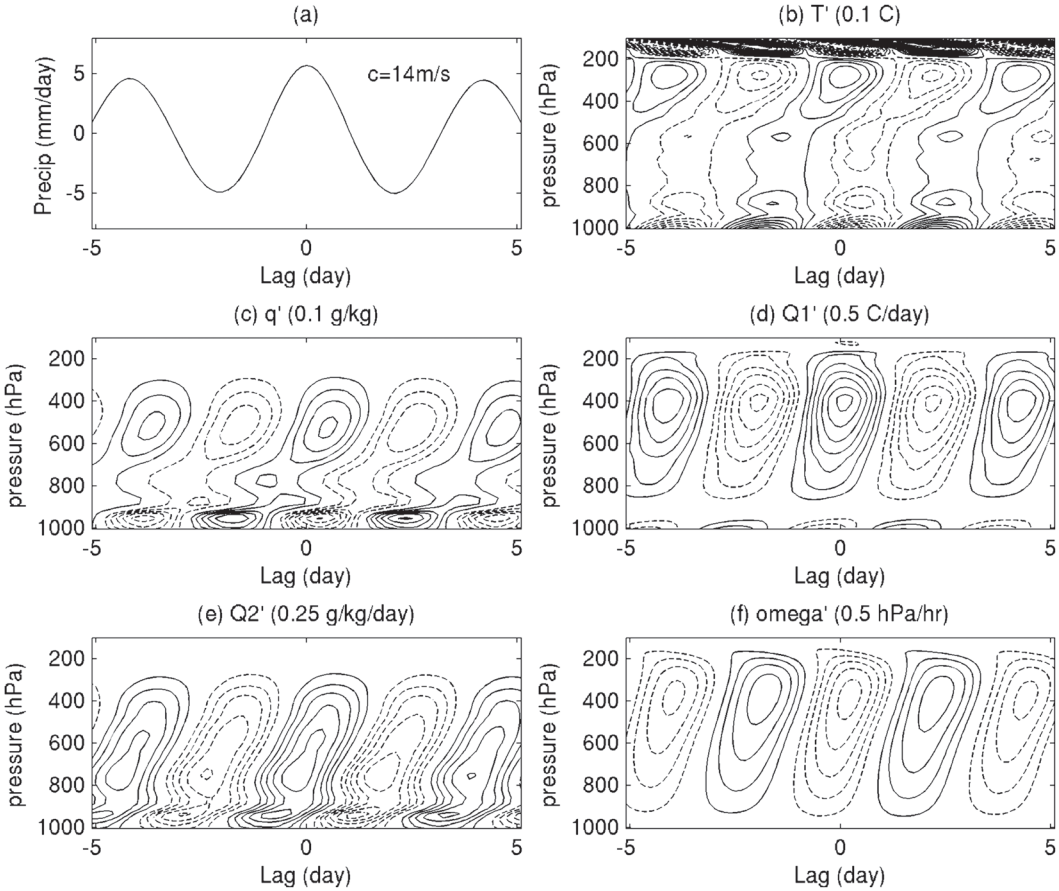


FIG. 6. As in Fig. 4 but for the control case with the RCE mean state. Contour intervals for (d),(e), and (f) are halved as the mean heating in the RCE case is weaker.

(a) A positive[3] temperature and/or specific humidity anomaly in the subcloud layer (the cloud base is around 930 hPa) is associated with anomalous cooling and drying in this layer and convective heating and drying in the free troposphere.

(b) With a warm anomaly above the subcloud layer, convection acts to reduce this anomaly and at the same time warm and moisten the subcloud layer (second row in Fig. 12). A warm temperature anomaly in the lower and middle troposphere reduces convective heating, not only locally but also in the layers above. This upward extension is more pronounced in the RCE case than in the TOGA COARE case. Its effects on the layers between the level of the perturbation and the subcloud layer tend to be small.

(c) The rate at which convection damps temperature anomalies decreases considerably from the lower troposphere to the middle and upper troposphere. For example, for the RCE case, the local cooling tendency associated with a warm anomaly of a given size peaking at 500 hPa is about 50% of that associated with a warm anomaly peaking at 800 hPa. The fraction drops to 30% for a warm anomaly peaking at 350 hPa. The decrease is somewhat smaller in the TOGA COARE case.

(d) A positive specific humidity anomaly in the free troposphere increases convective heating at and above that layer. At the same time, convection acts to remove this specific humidity anomaly and also cool and dry the subcloud layer. When normalized by the mean precipitation of their respective cases, the effects of free troposphere moisture variations appear stronger with the RCE mean state. The effects on the layers between the level of the perturbation and the subcloud layer tend to be small.

Features A and B simply state the well-known tendency for convection to adjust the atmosphere toward a convectively neutral state. Feature C, however, indicates

[3] We will only describe the responses to anomalies of one sign, noting the approximate linearity of the problem.

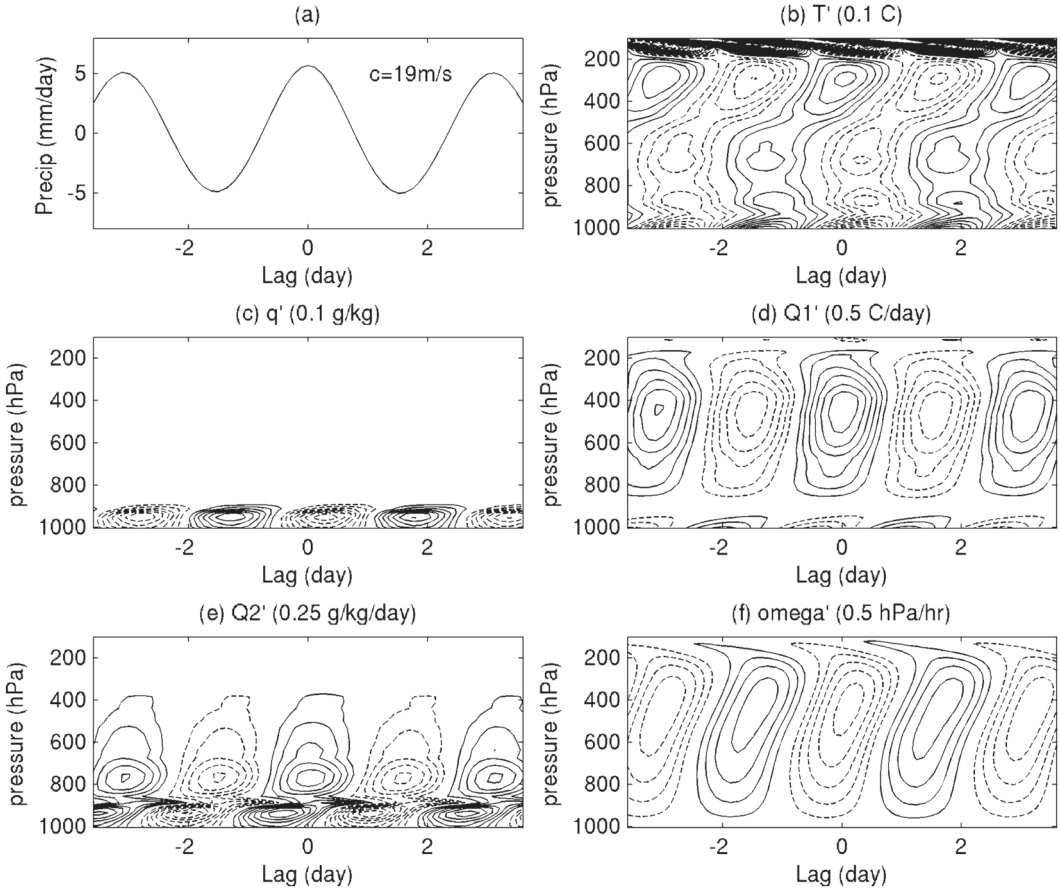


FIG. 7. As in Fig. 6 but for the case where domain-averaged specific humidity above 1 km is kept constant.

that the ability for convection to do so on a fast time scale decreases for a deeper layer. Features B and D show that both temperature and moisture perturbations at a range of heights can regulate the amount of convective heating at and above the level of the perturbations.

It is also informative to examine the eigenvalues and eigenvectors of the linear response function matrix **M**. Figures 14 and 15 show the *e*-folding time of all eigenvectors of **M** and the structure of the slowest decaying eigenmode, respectively, for the RCE case. In terms of the features that we shall discuss, results for the TOGA COARE case are similar. The slowest decaying mode has an *e*-folding time of ~15 days. This is distinctively longer than the *e*-folding times of the other eigenmodes, which range from ~1 h to ~2 days. The temperature profile of this eigenmode resembles a shift of a moist adiabatic profile (dashed line in Fig. 15a), and its specific humidity profile approximately conforms to the expected change with the relative humidity profile fixed to that of the reference state (dashed line in Fig. 15b). This eigenmode thus resembles the reference profile used in the Betts–Miller scheme (Betts 1986; Betts and Miller 1986). The long *e*-folding time scale is roughly that needed for the anomalous surface flux to remove the column-integrated moist static energy anomaly associated this eigenmode (recall that radiative cooling is held constant in the present study). The above behavior supports the notion that the cumulus ensemble adjusts the atmosphere toward the reference profiles assumed in the Betts–Miller scheme, and the reference profiles evolve more slowly through the adjustment of the column integrated moist static energy. However, Fig. 14 shows that adjustment toward the reference profiles is not uniformly fast with time scales of a couple of hours, as assumed in the Betts–Miller scheme. There are modes that do decay quickly with *e*-folding time of ~1 h, but there are also modes that decay much more slowly with *e*-folding time as long as 2 days, indicating a more complex adjustment process.

## 6. Comparison with a simple model

As an example of comparing CSRM results with toy/conceptual models, we shall consider the model of K08b,

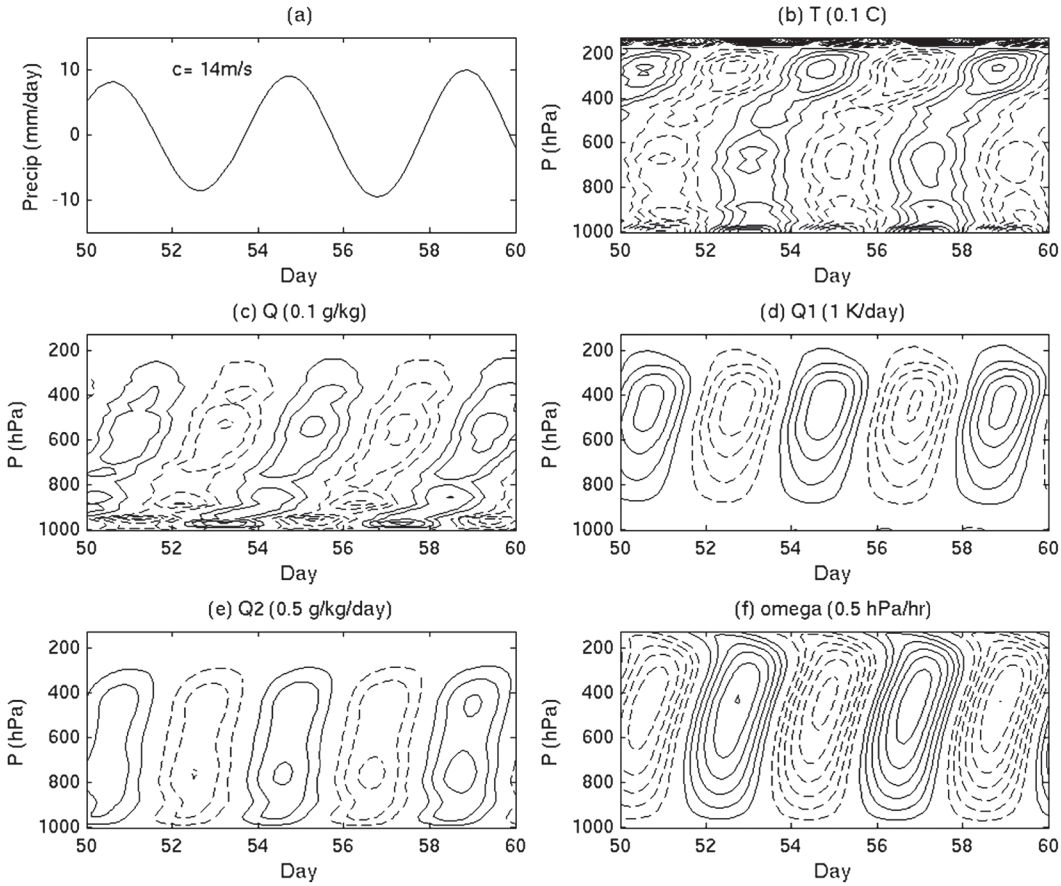


FIG. 8. Wave structures produced when the linear response functions, instead of the CSRM, are coupled with the large-scale gravity waves (horizontal wavelength is again 5000 km) for the control case with TOGA COARE background forcing: figure layout and contour intervals as in Fig. 4. A 20-day wave damping is used to control the wave growth.

which is part of a continuing effort in this field to construct models of minimal complexity to elucidate the basic dynamics of convectively coupled waves. Readers are referred to K08b and Andersen and Kuang (2008) for a detailed description and analysis of the model and its relation to previous models in the literature. Briefly, this model includes the first two baroclinic vertical modes, free or middle tropospheric moisture, and the subcloud

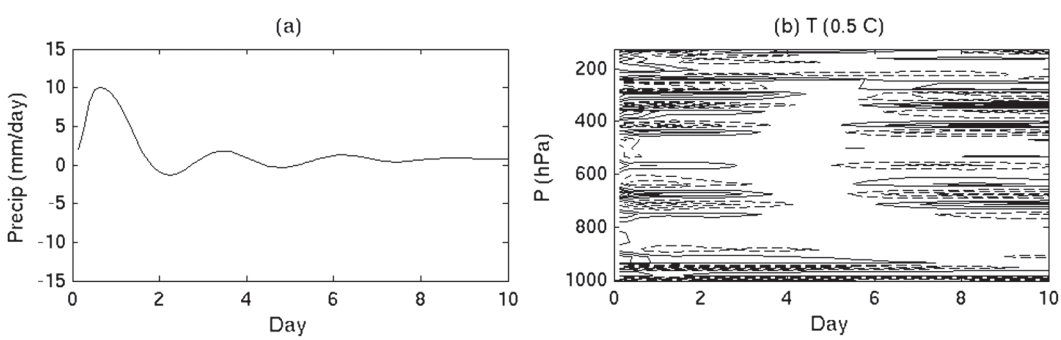


FIG. 9. Evolution of (a) precipitation and (b) temperature when the linear response functions, instead of the CSRM, are coupled with the large-scale gravity waves in the fixed free troposphere (>1 km) specific humidity case with the TOGA COARE background forcing. No wave damping is used.

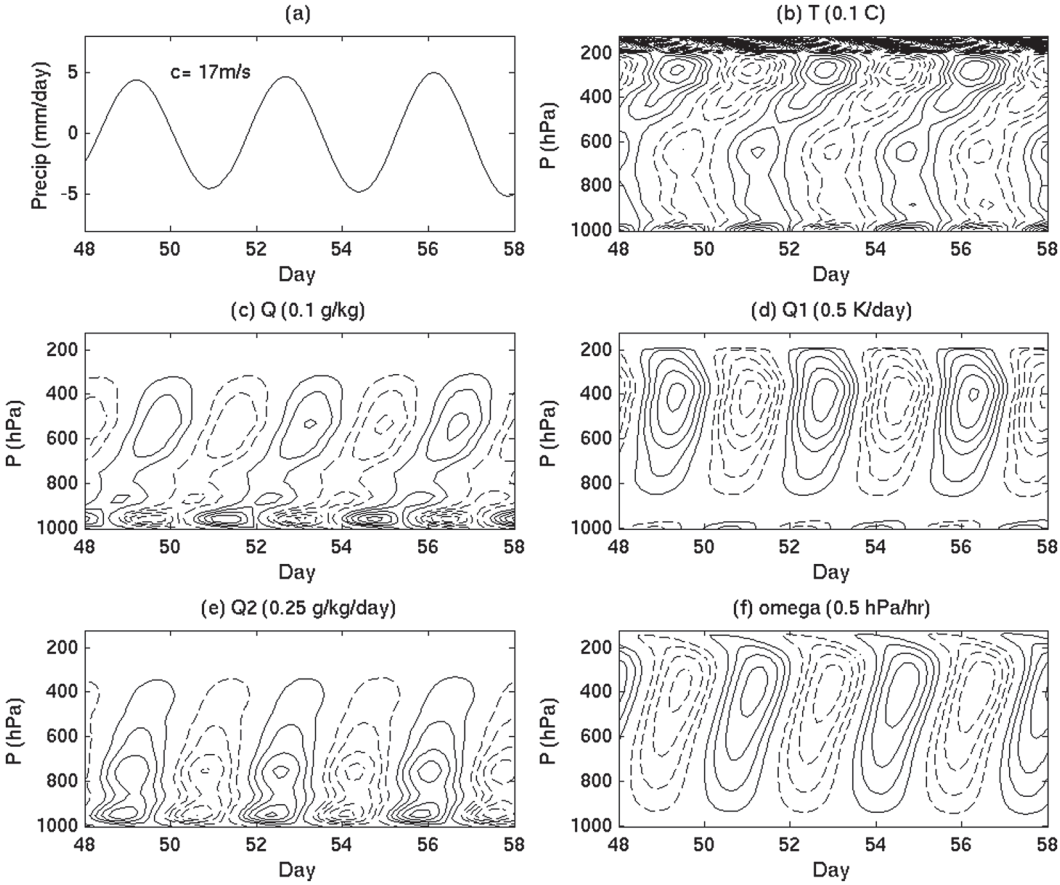


FIG. 10. As in Fig. 8 but for the RCE control case. Contour intervals for (d),(e), and (f) are halved compared to Fig. 8. A 1.7-day wave damping is used to neutralize the wave growth.

layer. The main novelty of this model is in its treatment of convection, which posits that convection maintains convective neutrality, not over the entire troposphere as in, for example, Emanuel et al. (1994), but over a shallower layer that extends only to the midtroposphere, and further that moisture variations in the free troposphere modulates the height of convection. These two treatments agree well with the constructed linear response functions, particularly features C[4] and D discussed in the previous section.

K08b identified two different instability mechanisms in their model. One is named the moisture-stratiform instability, where moisture variations in the free troposphere play a key role by regulating the depth of convective updrafts. The other instability, called direct stratiform instability, is the same as the stratiform instability identified in Mapes (2000, hereafter M00) and, as discussed in Andersen and Kuang (2008), is mathematically the same as the classical wave–conditional instability of the second kind, or wave–CISK (e.g., Lindzen 1974). The physical interpretation of how convection is regulated, however, is different between M00/K08b and the classical wave–CISK.

In K08b, the moisture-stratiform instability mechanism is present if free tropospheric moisture variations are effective in regulating the depth of convection. On the other hand, the direct stratiform instability is only present when the mean convective heating is top-heavy. The mathematical reason is the same as the well-known need for a top-heavy heating profile in studies of wave-CISK (e.g., Cho and Pendlebury 1997). Further experiments with the simple model of K08b show that, when direct stratiform instability is present, the overall growth

[4] The different control efficacies for temperature anomalies at different heights are also represented in the model of Mapes (2000) through its convectively available potential energy (CAPE) control and convective inhibition (CIN) control, where varying the relative importance of the two effectively varies the efficacies of the temperature control at different heights, and hence the depth of the convectively neutral layer. For a toy model, it seems that a shallower convectively neutral layer is a useful conceptual simplification.

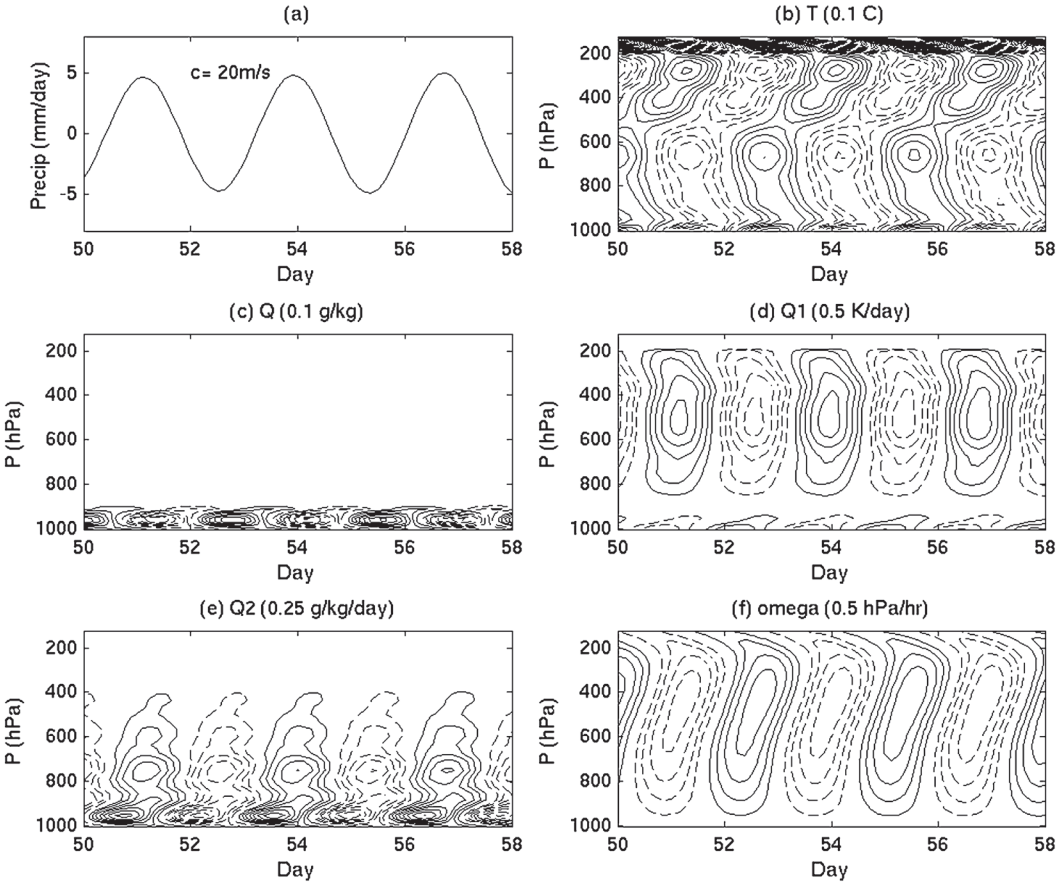


FIG. 11. As in Fig. 8 but for the RCE fixed free troposphere specific humidity case. Contour intervals for (d),(e), and (f) are halved. An 8-day wave damping is used to neutralize the wave growth.

rate is reduced when the effect of free tropospheric moisture variations on the depth of convection is removed. On the other hand, when the direct stratiform instability is absent, there are no unstable waves when effects of free tropospheric moisture variations are removed. The behavior of the simple model thus appears to agree with the above simulation results if one takes the RCE case to have a more top-heavy heating profile so that it contains the direct stratiform instability and the TOGA COARE case as having a less top-heavy heating profile, thus lacking such an instability.

Does the RCE case have a more top-heavy heating profile from wave modulation? K08b inferred this top heaviness indirectly from the mean convective heating profile. In CSRM experiments not presented here, we did find that more top-heavy mean convective heating profiles preferentially produce instability in the absence of free tropospheric moisture variations. However, comparing the mean convective heating profiles from RCE and TOGA COARE (Fig. 2c), one sees no evidence of a more top-heavy mean heating profile for the RCE case.

The linear response functions provide a more direct answer to the question above. Figure 12 shows that effects of temperature anomalies in the lower and mid-troposphere on convective heating do have a greater upward extension in the RCE case, corresponding to a more top-heavy heating profile in K08b (and M00). Tulich and Mapes (2010) also found this tendency of a more top-heavy response in convective heating to lower tropospheric temperature anomalies with a more weakly forced mean state. This more top-heavy response was found to increase the growth rate of large-scale convectively coupled waves and, for sufficiently top-heavy heating profiles, led to the direct stratiform instability, which does not require free tropospheric moisture variations (see Fig. 4d in K08b; a more top-heavy heating profile is represented by a larger $r_0$ parameter). Therefore, the reasons that the RCE case has stronger wave growth in the control run and possesses instability without variations in free troposphere specific humidity are, at a phenomenological level, captured by the simple model. There is also an indication that controls

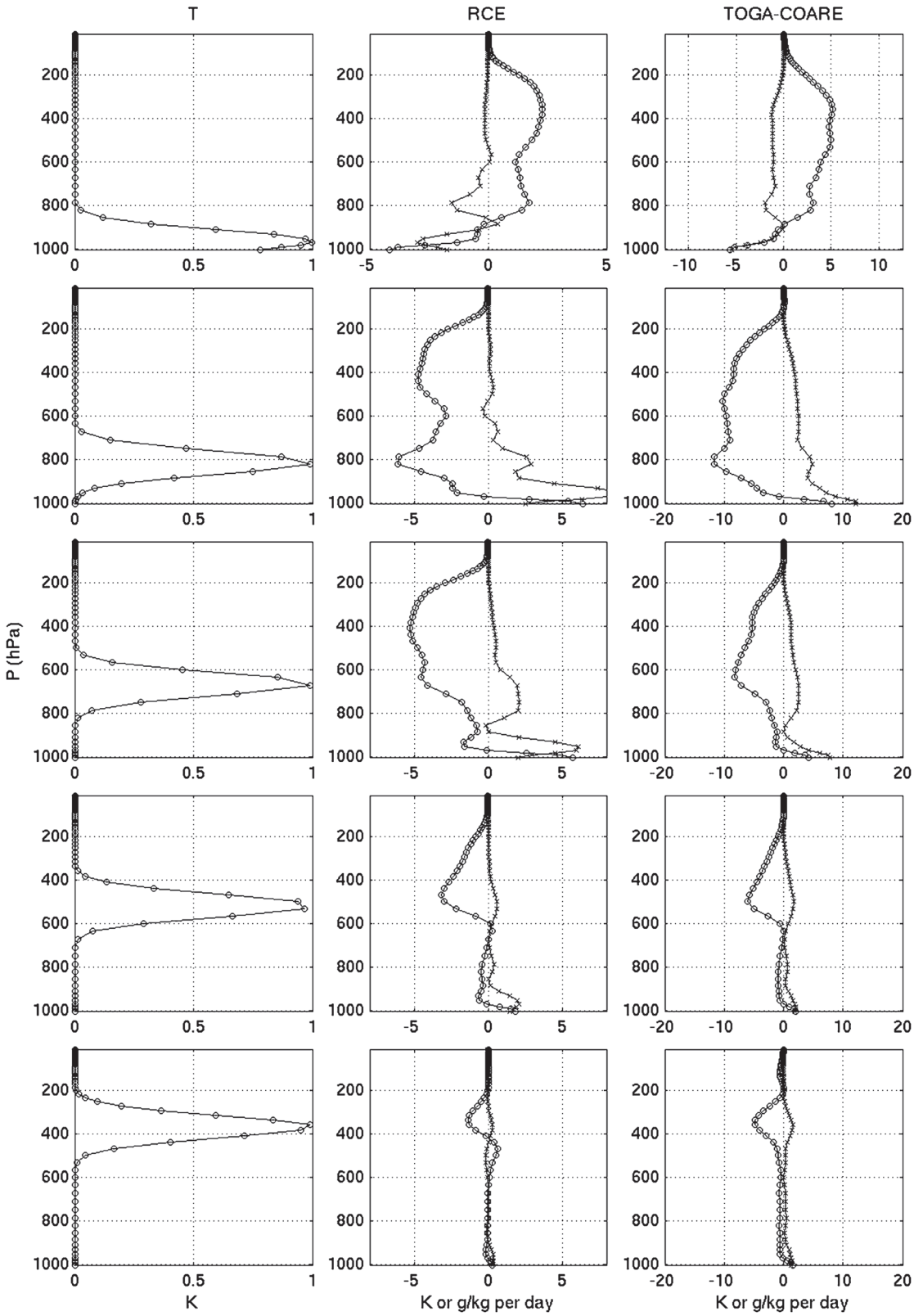


FIG. 12. (left) Anomalous convective heating (circles) and moistening (crosses) tendencies associated with warm anomalies and results for the (middle) RCE and (right) TOGA COARE cases. The tendency scales in the right column are 2.5 times those in the middle column.

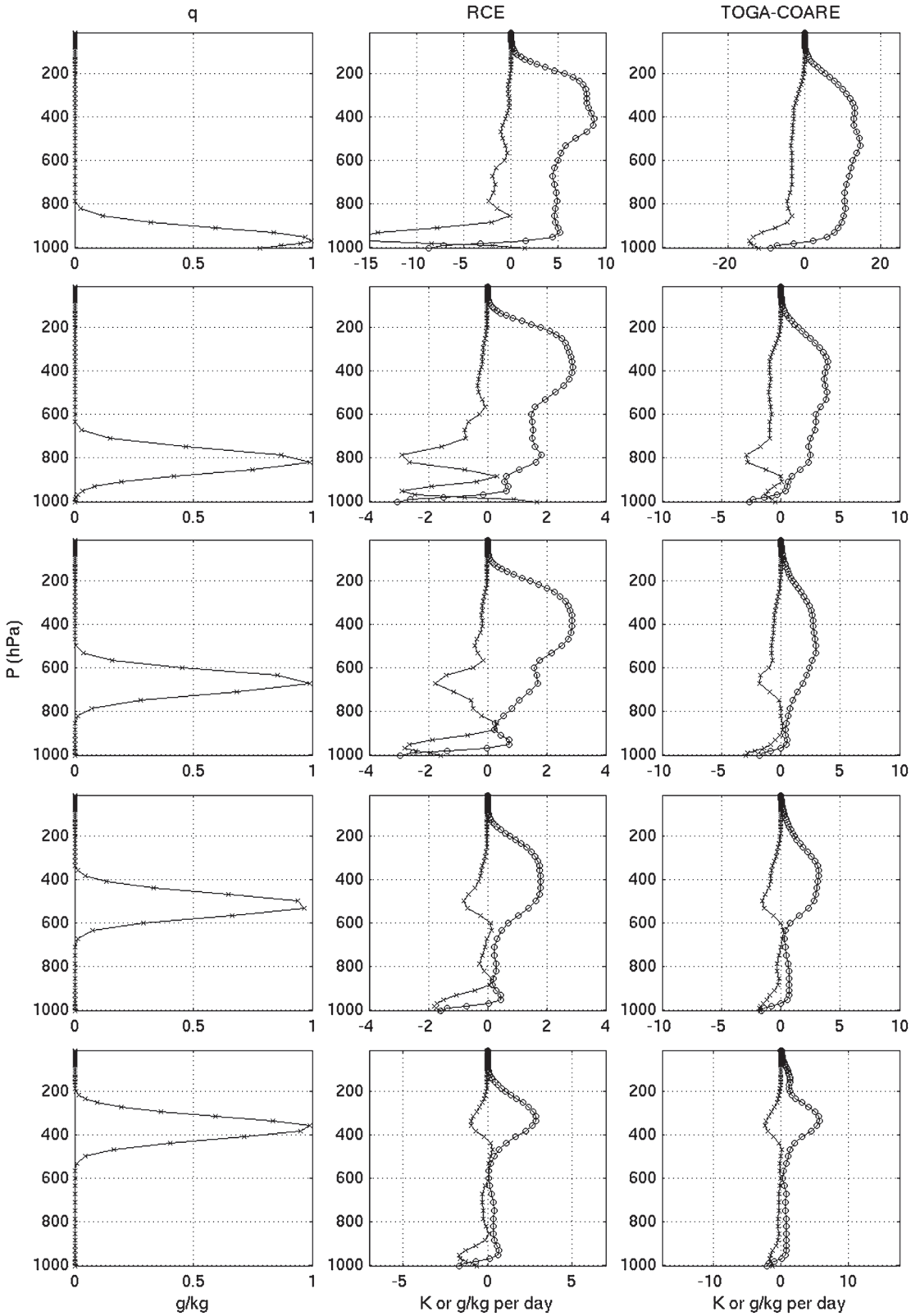


FIG. 13. As in Fig. 12 but for moisture anomalies peaking at a range of heights shown in the left column.

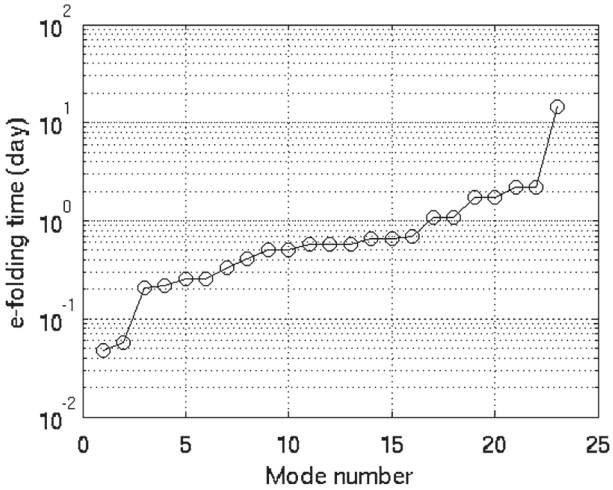


FIG. 14. The *e*-folding times of the eigenmodes of the linear response function matrix **M** for the RCE case.

by moisture variations are stronger in the RCE case (Fig. 13), which, represented by a larger $r_q$ parameter in K08, also leads to stronger instability (their Fig. 4e). Modifying these aspects of the linear response functions constructed here confirms these behaviors of the simple model. Since how these aspects affect the stability of the system is mainly mathematical, this confirmation is not surprising, but is nonetheless comforting. The above correspondence suggests that the simple model does provide the correct framework for interpreting the behavior of the CSRM and that the two instability mechanisms seen in the CSRM simulations are the same as those found in K08b.

The importance of the aforementioned characteristics of the response functions to the instability was analyzed mathematically in K08b, but may be appreciated more physically as the following. The weakened convective response to temperature anomalies in the upper troposphere (i.e., the convectively neutral layer being shallower) is necessary because it allows nonlocal control of convective heating there. Since convection tends to remove temperature anomalies locally (as evident in Fig. 12), a weak local response is more easily overwhelmed by nonlocal responses to perturbations elsewhere, namely specific humidity and temperature anomalies in the lower/middle troposphere. A stronger moisture control and/or a more top-heavy response to lower/middle troposphere temperature anomalies enhance the nonlocal response. This combination makes it possible for positive convective heating anomalies to occur in regions of positive temperature anomaly (and negative convective heating anomalies to occur in regions of negative temperature anomaly), leading to wave potential energy generation and wave growth. With the temperature/moisture controls taking the place of low-level moisture convergence, the basic mechanics at work is rather well illustrated in the work on wave-CISK (e.g., Raymond 1983).

## 7. Discussion

The response functions constructed here call into question the role of CIN control, traditionally referring to the strength of the weakly stable layer near the cloud base, in convectively coupled waves, as featured in some conceptual models (e.g., M00; Raymond and Fuchs 2007). Within the framework of M00, which has only two vertical modes, CIN control is little different from a lower tropospheric temperature control. However, in Raymond and Fuchs (2007), which is continuous in the vertical, CIN control emphasizes temperature control near the cloud base and neglects those above. As apparent in Fig. 12, the temperature controls are effective over a range of heights in the lower troposphere and stability in the thin layer near the cloud base is not anything special. In the context of the present CSRM, it can be directly verified that wave modulation of CIN does not have a key role by preventing convection from seeing wave modulations of temperature below, say, 1 km. We have done so by removing, at every time step, the cumulative effects of vertical temperature advection due to the large-scale waves below 1 km (which amounts to a correction to the domain mean temperature) before entering the integration of the CSRM. These effects are added back upon exiting the CSRM integration step. This approach preserves vertical temperature advection for the propagation of the large-scale wave while at the same time making wave modulation of temperature invisible over the specified height range to the cumulus ensemble. The cumulus ensemble still modulates temperature at all heights and these changes are visible to the large-scale wave. Such experiments with the CSRM and/or with the linear response functions, not presented here in figures, show that wave growth continues when wave modulation of temperature below 1 km is made invisible to the cumulus ensemble. On the other hand, there is no wave growth when wave modulation of temperature below 5 km is made invisible to the cumulus ensemble. These results confirm that what is relevant to convectively coupled waves is the general temperature control effect in the lower troposphere, not the stability over the thin layer near the cloud base.

The response functions constructed here are only phenomenological and require physical interpretations. Features A and B are straightforward consequences of convective adjustment. That temperature and moisture anomalies throughout the troposphere can act as controls on convection is consistent with the view that undiluted

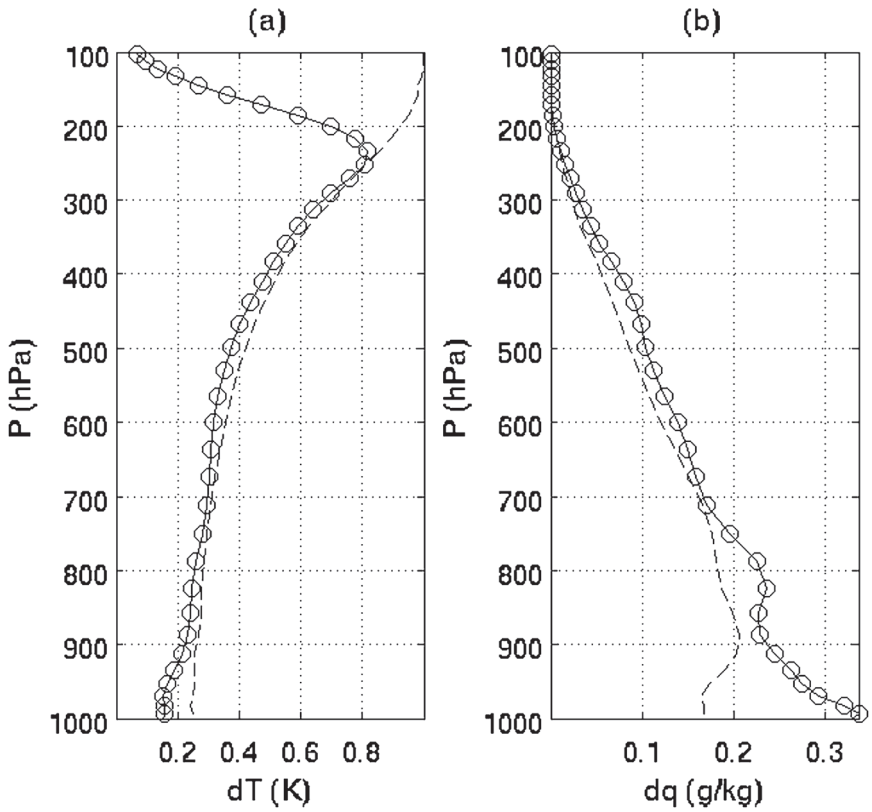


FIG. 15. (a) Temperature and (b) specific humidity components of the slowest decaying eigenmode for the RCE case. The *e*-folding time is ~15 days. The dashed line in (a) is the difference between two moist adiabats with $h/c_p$ of 347 and 348 K, where $h$ is the moist static energy and $c_p$ is the specific heat at constant pressure. The dashed line in (b) is the specific humidity change computed using the temperature change in (a) and the relative humidity profile of the reference state.

ascents are rare and unimportant in tropical oceanic convection: most, if not all, cloud parcels experience many mixing and buoyancy sorting events as they rise through the atmosphere. This view appears well supported by observations and CSRM simulations (e.g., Raymond and Blyth 1986; Zipser 2003; Kuang and Bretherton 2006; Romps and Kuang 2010). These mixing events with the environment modify the characteristics of the cloud parcels, making them susceptible to both temperature and moisture perturbations in the large-scale environmental conditions.

Many questions remain about the physical interpretation of the response functions. Why convective responses are stronger to lower tropospheric perturbations? Tulich and Mapes (2010) suggest small or negative mean updraft buoyancy in the lower troposphere as a potential reason. Investigations of this and other aspects of the convection are needed to answer this question. Why are the responses of convective heating to lower tropospheric temperature perturbations more top-heavy in RCE than in TOGA COARE? The reason for this difference is also not clear. Further diagnostics of the changes in the statistics of convection associated with the linear response functions are clearly needed for gaining more physical insight. It should also be interesting to compare the linear response functions constructed here with those from convective schemes to help diagnose the reason why many of them do not produce realistic convectively coupled waves. Constructing the linear response functions should be much easier for a parameterization because, unlike the CSRM, a typical cumulus parameterization has no stochastic noise. If the scheme predicts convective tendencies solely based on the current time step large-scale sounding, that is, no memory, as in Eq. (1), one can simply impose a perturbation to the sounding and compute the convective tendencies. Last, the apparent dependence of convectively coupled waves on the mean state as simulated by this CSRM is intriguing. It would be interesting to test this prediction with more refined observational analyses.

## 8. Summary

We have presented a method to compute linear response functions from a CSRM. The approach is to apply, one at a time, a set of steady perturbation forcings to the CSRM and record the equilibrium responses in the state vector. The responses are found to be approximately linear for perturbation sizes relevant to the observed waves. With a sufficiently complete set of perturbation forcings, we can derive the anomalous convective tendencies that are in statistical equilibrium with given anomalies in the state vector. For the problem of coupling with large-scale waves, such tendencies are more relevant than responses to perturbations suddenly introduced to the CSRM because in these waves the state vectors vary slowly compared to the response time of the cumulus ensemble. We applied the method to two different mean state conditions for which the CSRM, when coupled with large-scale 2D gravity waves, exhibits interestingly different behavior. In the case forced with the large-scale vertical velocity profile taken from the TOGA COARE experiment, convectively coupled waves develop in the control simulation but disappear when free troposphere specific humidity variations are removed. With the RCE mean state, growth of convectively coupled waves is stronger in the control, and convectively coupled waves continue to develop even when free troposphere specific humidity is kept constant. Despite the many approximations made during the construction (e.g., linearity, incomplete set of basis functions), the linear response functions were able to reproduce these behaviors of the CSRM with some quantitative accuracy. Comparing the response functions with the treatment of convection in the simple model of K08b indicates that they are generally consistent, lending confidence that the moisture-stratiform instability and the direct stratiform instability (the same as the stratiform instability in M00) identified in K08b provide the correct explanation to the instability seen in the CSRM simulations.

*Acknowledgments.* The author thanks Marat Khairoutdinov for making the SAM model available, Kerry Emanuel for encouragement, Brian Mapes, Kerry Emanuel, and Dave Raymond for discussions on convectively coupled waves, and David Romps, Chris Walker, Brian Mapes, and two anonymous reviewers for their thoughtful suggestions that helped to improve the presentation of this paper. This research was partially supported by the Office of Biological and Environmental Research of the U.S. Department of Energy under Grant DE-FG02–08ER64556 as part of the Atmospheric Radiation Measurement Program and NSF Grant ATM-0754332. The Harvard Odyssey cluster provided much of the computing resources for this study.

## APPENDIX

### Comparison with the Initial Perturbation Approach

In this appendix, we briefly compare evolutions of the state vector from the initial perturbation approach and those computed using the linear response functions. In Figs. A1 and A2, we present the time evolution over a 12-h period after anomalies are suddenly introduced to the state vector. The CSRM has been run to a statistical equilibrium state when the anomalies are introduced. The model and experimental setup are the same as in the RCE case except a 384 km $\times$ 384 km domain is used to reduce the noisiness in the domain-averaged $T$ and $q$ (or the number of ensembles needed to achieve a certain signal-to-noise ratio). The results shown are averages of 100 ensemble members, each starting from a different time (separated by 12 h) in a long control (unperturbed) run. In the experiments, the initial perturbations take the same shape as those in Figs. 12 and 13, with peak values of 0.2 K for temperature and 0.2 g kg$^{-1}$ for specific humidity, and the responses are linear to a good approximation for perturbations of these sizes (not shown). In Figs. A1 and A2, the results are normalized to given initial temperature perturbations with peak values of 1 K and initial specific humidity perturbations with peak values of 1 g kg$^{-1}$. In Figs. A3 and A4, we show the results computed using the linear response functions as $\mathbf{x}_0 \exp(-Mt)$, where $\mathbf{x}_0$ is the initial perturbation. One sees general agreement between the two approaches except that the evolutions in Figs. A3 and A4 are delayed by a couple of hours relative to those in Figs. A1 and A2, a consequence of the convective response time.

It may appear at first sight that the responses in Figs. A1 and A2 have more direct physical meaning than those in Figs. A3 and A4, as they correspond to the actual evolution of anomalies suddenly added to the state vector. Our experience has been that the initial perturbation approach can give useful insights to how convection adjusts to sudden perturbations, whereas with the prescribed forcing approach one can more easily obtain the accuracy needed to reproduce the coupled waves simulated by the full CSRM, where temperature/moisture anomalies vary slowly instead of being introduced suddenly. The ability to reproduce the behavior of the full CSRM allows us to ascertain that the linear response functions provide an adequate representation of the full CSRM, which is an important part of the present study.

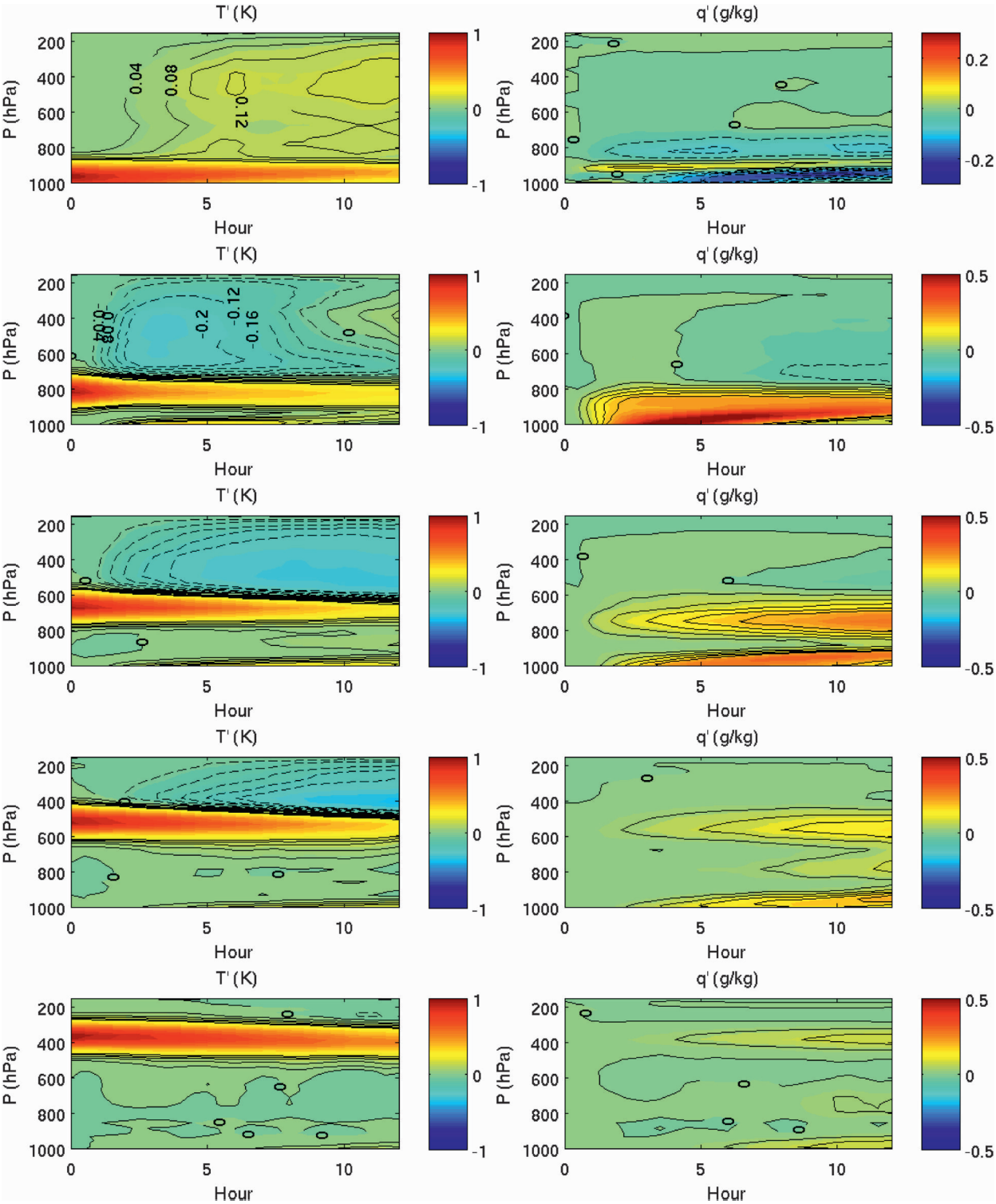


FIG. A1. Evolutions of (left) temperature and (right) specific humidity anomalies after initial temperature perturbations are introduced at a range of heights at hour 0. The initial temperature perturbations have the same shapes as those shown in the left column of Fig. 12 and have peak magnitudes of 0.2 K in the simulations but are normalized to 1 K in the plots.

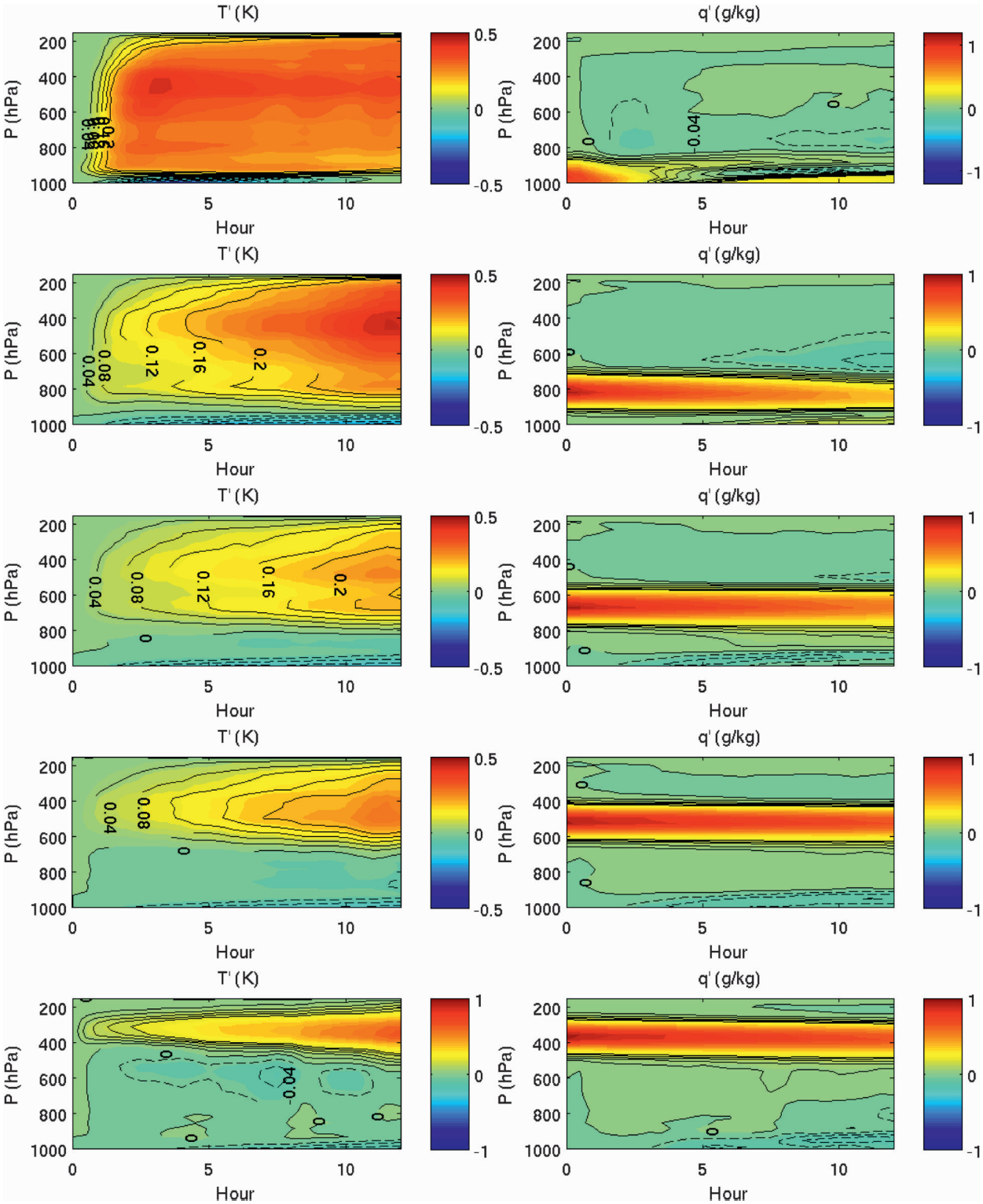


FIG. A2. As in Fig. 14 but for initial specific humidity perturbations. The initial temperature perturbations have the same shapes as those in the left column of Fig. 13 and have peak magnitudes of 0.2 g kg$^{-1}$ in the simulations but are normalized to 1 g kg$^{-1}$ in the plots.

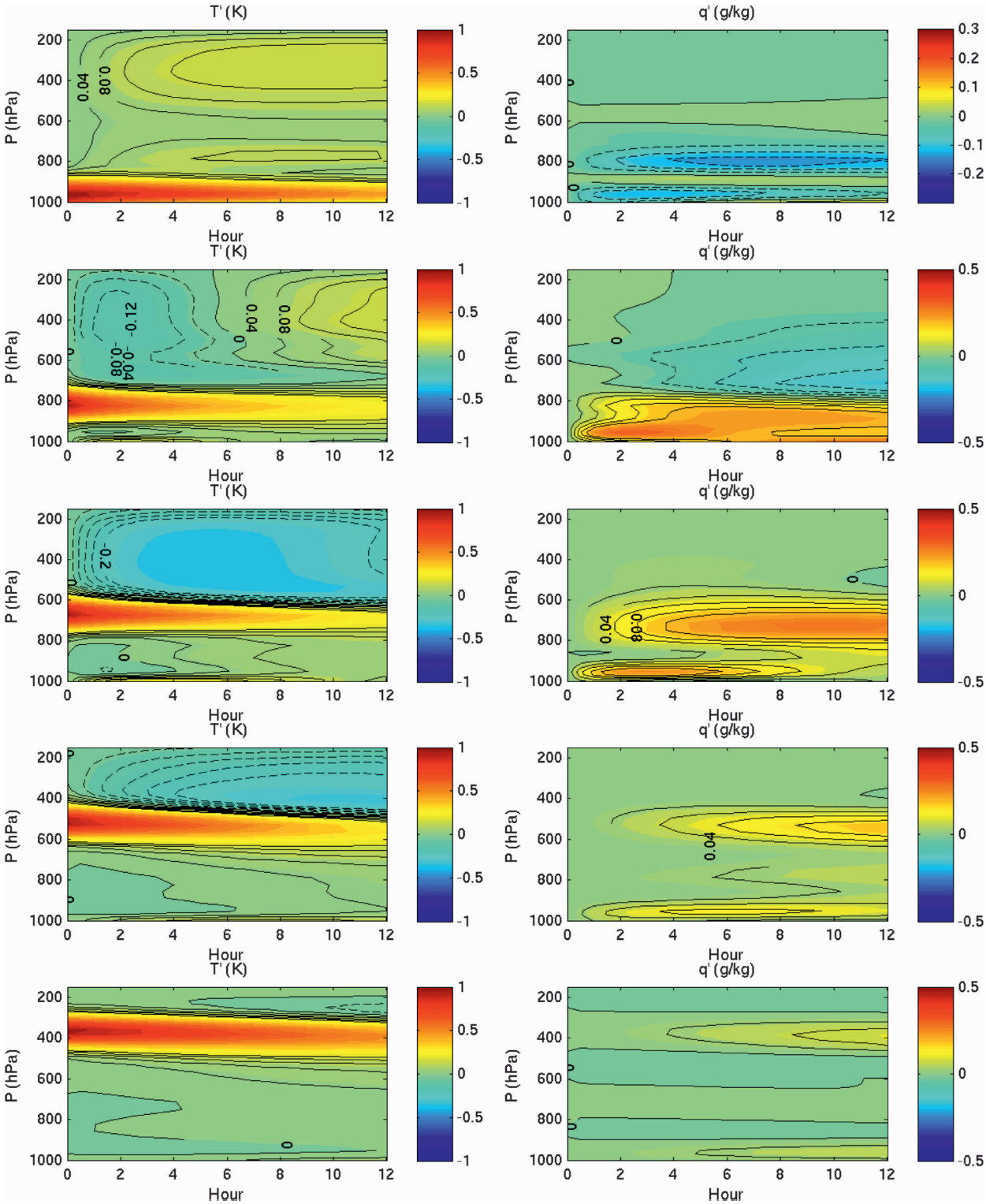


FIG. A3. Same evolution as in Fig. 14 but produced using the linear response functions as $\mathbf{x}_0 \exp(-Mt)$.

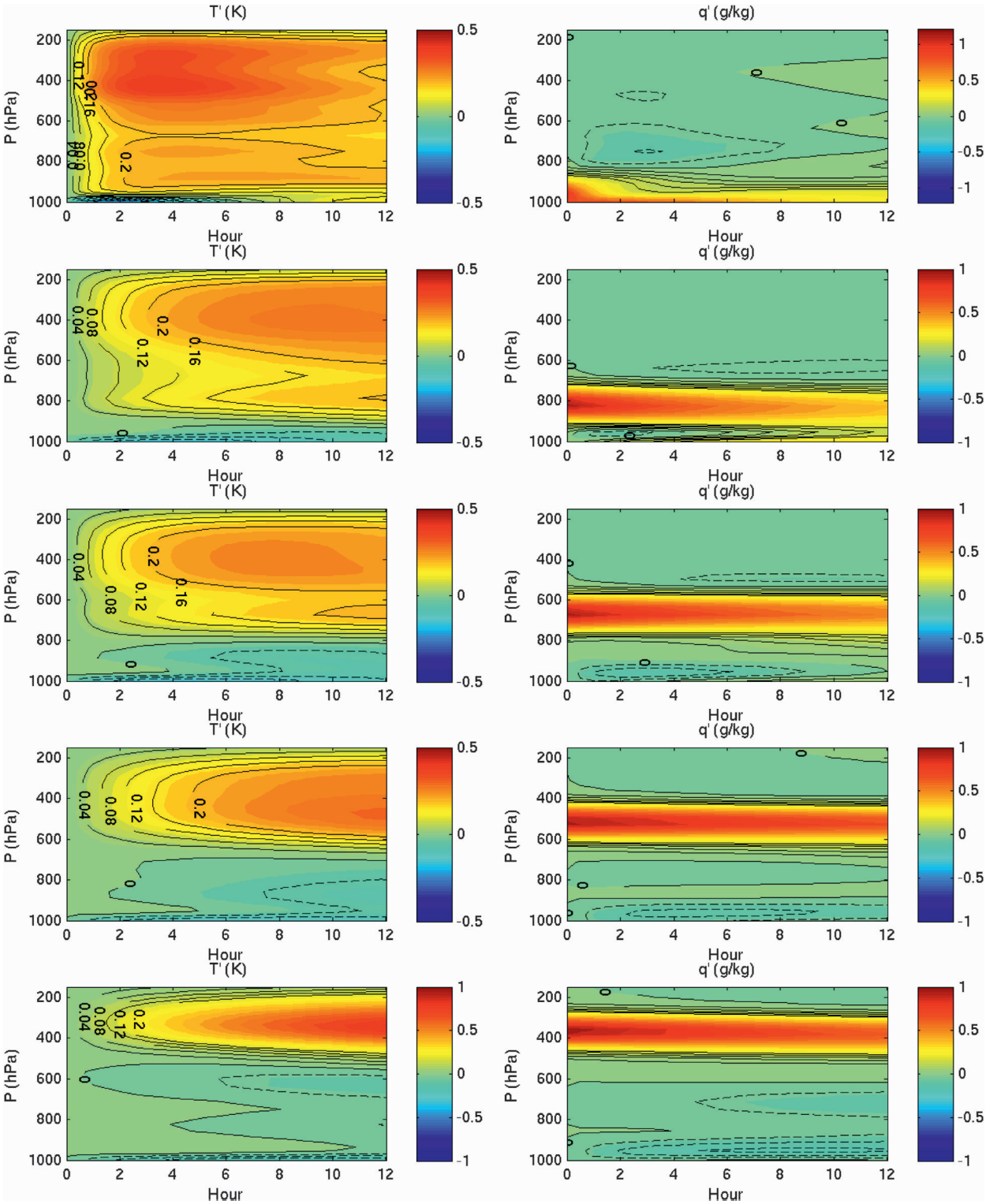


FIG. A4. As in Fig. A1 but for initial specific humidity perturbations.

## REFERENCES


Andersen, J. A., and Z. Kuang, 2008: A toy model of the instability in the equatorially trapped convectively coupled waves on the equatorial beta plane. *J. Atmos. Sci.,* **65,** 3736–3757.

Betts, A. K., 1986: A new convective adjustment scheme. Part I: Observational and theoretical basis. *Quart. J. Roy. Meteor. Soc.,* **112,** 677–691.

——, and M. J. Miller, 1986: A new convective adjustment scheme. Part II: Single column tests using GATE wave, BOMEX, ATEX and arctic air-mass data sets. *Quart. J. Roy. Meteor. Soc.,* **112,** 693–709.

Cho, H.-R., and D. Pendlebury, 1997: Wave CISK of equatorial waves and the vertical distribution of cumulus heating. *J. Atmos. Sci.,* **54,** 2429–2440.

Derbyshire, S. H., I. Beau, P. Bechtold, J.-Y. Grandpeix, J.-M. Piriou, J.-L. Redelsperger, and P. M. M. Soares, 2004: Sensitivity of moist convection to environmental humidity. *Quart. J. Roy. Meteor. Soc.,* **130,** 3055–3079.

Emanuel, K. A., 1987: An air–sea interaction model of intraseasonal oscillations in the tropics. *J. Atmos. Sci.,* **44,** 2324–2340.

——, J. D. Neelin, and C. S. Bretherton, 1994: On large-scale circulations in convecting atmospheres. *Quart. J. Roy. Meteor. Soc.,* **120,** 1111–1143.

Fuchs, Z., and D. J. Raymond, 2002: Large-scale modes of a nonrotating atmosphere with water vapor and cloud–radiation feedbacks. *J. Atmos. Sci.,* **59,** 1669–1679.

Grabowski, W. W., and M. W. Moncrieff, 2001: Large-scale organization of tropical convection in two-dimensional explicit numerical simulations. *Quart. J. Roy. Meteor. Soc.,* **127,** 445–468.

——, and ——, 2004: Moisture–convection feedback in the tropics. *Quart. J. Roy. Meteor. Soc.,* **130,** 3081–3104.

Haertel, P. T., and G. N. Kiladis, 2004: Dynamics of 2-day equatorial waves. *J. Atmos. Sci.,* **61,** 2707–2721.

Khairoutdinov, M. F., and D. A. Randall, 2003: Cloud resolving modeling of the ARM summer 1997 IOP: Model formulation, results, uncertainties, and sensitivities. *J. Atmos. Sci.,* **60,** 607–625.

Khouider, B., and A. J. Majda, 2006: A simple multicloud parameterization for convectively coupled tropical waves. Part I: Linear analysis. *J. Atmos. Sci.,* **63,** 1308–1323.

Kiladis, G. N., M. C. Wheeler, P. T. Haertel, K. H. Straub, and P. E. Roundy, 2009: Convectively coupled equatorial waves. *Rev. Geophys.,* **47,** RG2003, doi:10.1029/2008RG000266.

Kuang, Z., 2008a: Modeling the interaction between cumulus convection and linear gravity waves using a limited-domain cloud system–resolving model. *J. Atmos. Sci.,* **65,** 576–591.

——, 2008b: A moisture-stratiform instability for convectively coupled waves. *J. Atmos. Sci.,* **65,** 834–854.

——, and C. Bretherton, 2006: A mass flux scheme view of a high-resolution simulation of a transition from shallow to deep cumulus convection. *J. Atmos. Sci.,* **63,** 1895–1909.

——, P. N. Blossey, and C. S. Bretherton, 2005: A new approach for 3D cloud-resolving simulations of large-scale atmospheric circulation. *Geophys. Res. Lett.,* **32,** L02809, doi:10.1029/2004GL021024.

Lindzen, R. S., 1974: Wave-CISK in the tropics. *J. Atmos. Sci.,* **32,** 156–179.

Mapes, B. E., 2000: Convective inhibition, subgrid-scale triggering energy, and stratiform instability in a toy tropical wave model. *J. Atmos. Sci.,* **57,** 1515–1535.

Nasuno, T., H. Tomita, S. Iga, H. Miura, and M. Satoh, 2008: Convectively coupled equatorial waves simulated on an aquaplanet in a global nonhydrostatic experiment. *J. Atmos. Sci.,* **65,** 1246–1265.

Neelin, J. D., and J.-Y. Yu, 1994: Modes of tropical variability under convective adjustment and the Madden–Julian oscillation. Part I: Analytical results. *J. Atmos. Sci.,* **51,** 1876–1894.

——, I. M. Held, and K. H. Cook, 1987: Evaporation–wind feedback and low-frequency variability in the tropical atmosphere. *J. Atmos. Sci.,* **44,** 2341–2348.

Peters, M. E., and C. S. Bretherton, 2006: Structure of tropical variability from a vertical mode perspective. *Theor. Comput. Fluid Dyn.,* **20,** 501–524.

Raymond, D. J., 1983: Wave-CISK in mass flux form. *J. Atmos. Sci.,* **40,** 2561–2574.

——, and A. M. Blyth, 1986: A stochastic mixing model for nonprecipitating cumulus clouds. *J. Atmos. Sci.,* **43,** 2708–2718.

——, and Z. Fuchs, 2007: Convectively coupled gravity and moisture modes in a simple atmospheric model. *Tellus,* **59A,** 627–640.

Redelsperger, J. L., D. B. Parsons, and F. Guichard, 2002: Recovery processes and factors limiting cloud-top height following the arrival of a dry intrusion observed during TOGA COARE. *J. Atmos. Sci.,* **59,** 2438–2457.

Romps, D. M., and Z. Kuang, 2010: Do undiluted convective plumes exist in the upper tropical troposphere? *J. Atmos. Sci.,* **67,** 468–484.

Straub, K. H., and G. N. Kiladis, 2002: Observations of a convectively coupled Kelvin wave in the eastern Pacific ITCZ. *J. Atmos. Sci.,* **59,** 30–53.

Takayabu, Y. N., 1994: Large-scale cloud disturbances associated with equatorial waves. Part I: Spectral features of the cloud disturbances. *J. Meteor. Soc. Japan,* **72,** 433–449.

Takemi, T., O. Hirayama, and C. H. Liu, 2004: Factors responsible for the vertical development of tropical oceanic cumulus convection. *Geophys. Res. Lett.,* **31,** L11109, doi:10.1029/2004GL020225.

Tompkins, A. M., and G. C. Craig, 1998: Time-scales of adjustment to radiative-convective equilibrium in the tropical atmosphere. *Quart. J. Roy. Meteor. Soc.,* **124,** 2693–2713.

Tulich, S. N., and B. E. Mapes, 2008: Multiscale convective wave disturbances in the tropics: Insights from a two-dimensional cloud-resolving model. *J. Atmos. Sci.,* **65,** 140–155.

——, and ——, 2010: Transient environmental sensitivities of explicitly simulated tropical convection. *J. Atmos. Sci.,* **67,** 957–974.

——, D. Randall, and B. Mapes, 2006: Vertical-mode and cloud decomposition of large-scale convectively coupled gravity waves in a two-dimensional cloud-resolving model. *J. Atmos. Sci.,* **64,** 1210–1229.

Webster, P. J., and R. Lukas, 1992: TOGA COARE—The Coupled Ocean Atmosphere Response Experiment. *Bull. Amer. Meteor. Soc.,* **73,** 1377–1416.

Wheeler, M., and G. N. Kiladis, 1999: Convectively coupled equatorial waves: Analysis of clouds and temperature in the wavenumber–frequency domain. *J. Atmos. Sci.,* **56,** 374–399.

Zipser, E. J., 2003: Some views on hot towers after 50 years of tropical field programs and two years of TRMM data. *Cloud Systems, Hurricanes, and the Tropical Rainfall Measuring Mission (TRMM)—A Tribute to Dr. Joanne Simpson, Meteor. Monogr.,* No. 51, Amer. Meteor. Soc., 50–59.